THE JOURNAL OF BIOLOGICAL CHEMISTRY VOL. 288, NO. 41, pp. 29911–29922, October 11, 2013

Characterization of a Highly Efficient Blue-shifted Channelrhodopsin from the Marine Alga *Platymonas subcordiformis*[*] [S]

Received for publication, July 25, 2013, and in revised form, August 16, 2013 Published, JBC Papers in Press, August 30, 2013, DOI 10.1074/jbc.M113.505495

Elena G. Govorunova[‡], Oleg A. Sineshchekov[‡], Hai Li[‡], Roger Janz[§], and John L. Spudich[‡1]

From the [‡]Department of Biochemistry & Molecular Biology, Center for Membrane Biology and the [§]Department of Neurobiology and Anatomy, University of Texas Medical School, Houston, Texas 77030

Background: Channelrhodopsins are algal phototaxis receptors used in optogenetics.
Results: Channel activity and photochemistry of a new channelrhodopsin (*Ps*ChR) are characterized.
Conclusion: Blue-shifted *Ps*ChR has ~3-fold greater unitary conductance, faster recovery from excitation, and higher sodium selectivity than channelrhodopsin 2 from *Chlamydomonas*.
Significance: These properties of *Ps*ChR facilitate further analysis of light-gated channel function and are potentially useful for optogenetics.

Rhodopsin photosensors of phototactic algae act as light-gated cation channels when expressed in animal cells. These proteins (channelrhodopsins) are extensively used for millisecond scale photocontrol of cellular functions (optogenetics). We report characterization of *Ps*ChR, one of the phototaxis receptors in the alga *Platymonas* (*Tetraselmis*) *subcordiformis*. *Ps*ChR exhibited ~3-fold higher unitary conductance and greater relative permeability for Na^+ ions, as compared with the most frequently used channelrhodopsin-2 from *Chlamydomonas reinhardtii* (*Cr*ChR2). Photocurrents generated by *Ps*ChR in HEK293 cells showed lesser inactivation and faster peak recovery than those by *Cr*ChR2. Their maximal spectral sensitivity was at 445 nm, making *Ps*ChR the most blue-shifted channelrhodopsin so far identified. The λ_{max} of detergent-purified *Ps*ChR was 437 nm at neutral pH and exhibited red shifts (pK_a values at 6.6 and 3.8) upon acidification. The purified pigment undergoes a photocycle with a prominent red-shifted intermediate whose formation and decay kinetics match the kinetics of channel opening and closing. The rise and decay of an M-like intermediate prior to formation of this putative conductive state were faster than in *Cr*ChR2. *Ps*ChR mediated sufficient light-induced membrane depolarization in cultured hippocampal neurons to trigger reliable repetitive spiking at the upper threshold frequency of the neurons. At low frequencies spiking probability decreases less with *Ps*ChR than with *Cr*ChR2 because of the faster recovery of the former. Its blue-shifted absorption enables optogenetics at wavelengths even below 400 nm. A combination of characteristics makes *Ps*ChR important for further research on structure-function relationships in ChRs and potentially useful for optogenetics, especially for combinatorial applications when short wavelength excitation is required.

Photomotility responses in green flagellate algae are mediated by retinylidene proteins with shared sequence homology to other microbial rhodopsins (for review see Refs. 1 and 2). Their photoexcitation leads to depolarization of the algal plasma membrane (3–5), which initiates a signaling cascade that eventually brings about correction of the cell swimming path according to the direction of light. An incisive method to probe rhodopsin-mediated light signaling in phototactic algae is measurement of photoinduced electrical signals in cell suspensions (6). With this assay, photoreceptor currents were detected in a variety of species, and their analysis revealed a dual receptor sensory system common for all tested algae with intrachloroplast eyespots (reviewed in Ref. 1).

Algal sensory rhodopsins demonstrate light-gated cation channel activity when heterologously expressed in animal cells and are therefore called "channelrhodopsins" (ChRs)[2] (7, 8). They predominantly conduct protons but are also permeable for mono- and divalent metal cations. ChRs are widely used for control of neuronal firing, muscle contraction and other cellular processes by light ("optogenetics"; for review see Refs. 9–12). High efficiency and temporal precision are required of optogenetic tools, especially when low stimulus intensities or high stimulation frequencies are desirable, but the ChRs known so far are not ideal in these respects. Their performance has been somewhat increased by molecular engineering, *e.g.*, by point mutations and/or construction of chimeras between different natural sequences (reviewed by Refs. 13 and 14). For example, the H134R and T159C mutants of ChR2 from *Chlamydomonas reinhardtii* generate ~3- and ~10-fold larger currents, respectively, as compared with the wild type, but this gain in amplitude is accompanied by a loss in rates of current rise

* This work was supported, in whole or in part, by National Institutes of Health Grants R01GM027750 and R21MH098288. This work was also supported by the Hermann Eye Fund and Endowed Chair AU-0009 from the Robert A. Welch Foundation.
[S] This article contains supplemental Fig. S1.
[1] To whom correspondence should be addressed: Center for Membrane Biology, Dept. of Biochemistry & Molecular Biology, University of Texas Medical School, 6431 Fannin St., Houston, TX 77030. Tel.: 713-500-5473; E-mail: john.l.spudich@uth.tmc.edu.

[2] The abbreviations used are: ChR, channelrhodopsin; *Ps*ChR, *P. subcordiformis* channelrhodopsin; *Cr*ChR, *C. reinhardtii* channelrhodopsin; *Mv*ChR1, *M. viride* channelrhodopsin; TM, transmembrane; BR, bacteriorhodopsin.

and decay (15, 16). C1V1, a recently developed chimera of *Cr*ChR1 and *Vc*ChR1, produces 3-fold larger currents but retains extremely slow decay kinetics characteristic of parental *Vc*ChR1, which could be partially improved by introducing a combination of point mutations (17, 18).

A complementary strategy for optimization and extension of the optogenetic toolkit is searching for natural ChR variants in other algae. Previously we briefly reported cloning a new sequence, designated *Ps*ChR, from the phototactic alga *Platymonas* (*Tetraselmis*) *subcordiformis* (19). In this study, we show that *Ps*ChR is one of the two receptors for phototaxis in this alga. We also present a detailed analysis of its photoelectric activity in cultured animal cells and characterize optical properties of the purified pigment by spectroscopy and flash photolysis.

Here we report that currents generated by *Ps*ChR in HEK293 cells show higher amplitude, smaller inactivation, and faster peak recovery than those generated by *Cr*ChR2, the molecule of choice in most optogenetic studies, whereas their kinetics is similarly fast. The higher current amplitude of *Ps*ChR is due to its higher unitary conductance, as estimated by stationary noise analysis. *Ps*ChR shows greater relative permeability for Na^+ ions over protons, as compared with *Cr*ChR2, which in optogenetic applications could minimize undesirable pH changes in the neuronal cytoplasm. We find that *Ps*ChR expressed in cultured hippocampal neurons evokes action potentials by short light pulses delivered at frequencies up to 50 Hz, which is the upper limit of functioning for this type of neuron (20). Light control of spiking on the time scale of seconds was more reliable with *Ps*ChR than with *Cr*ChR2, because of the faster recovery of *Ps*ChR from excitation. With its maximum sensitivity at 445 nm, *Ps*ChR is the most blue-shifted channelrhodopsin found so far, ideally suited for coupling with long wavelength absorbing rhodopsin pumps for light-regulated bidirectional control of the membrane potential (21–23) or with fluorescent voltage- or Ca^{2+}-sensitive probes (24–27), which are becoming increasingly popular.

EXPERIMENTAL PROCEDURES

Photocurrents in Native Cells—P. (Tetraselmis) subcordiformis was obtained from the UTEX Culture Collection of Algae (strain 71) and grown in modified artificial seawater medium (28) under 16-h light/8-dark cycle (light: 2,000 lux). Photoelectric currents in the algal cells were measured with the population assay invented earlier (6). The method takes advantage of the directional sensitivity of the photoreceptor antenna complex in flagellates. Two platinum wires immersed in a cell suspension pick up an electrical current generated in response to a unilateral excitation flash from a Vibrant HE 355II Tunable Laser (OPOTEK Inc., Carlsbad, CA) set at desired wavelengths. To decrease the current noise, cells from a 2-week culture were harvested and resuspended in the measuring medium of a lower ionic strength (0.5 mM $CaCl_2$ and 40 mM NaCl). The signal was amplified by a low noise current amplifier (model 428; Keithley Instruments, Cleveland, OH) and digitized by a Digidata 1322A supported by pClamp 10 software (both from Molecular Devices, Union City, CA).

Whole Cell Patch Clamp Measurements in HEK293 Cells— The mammalian expression vector that contained *Ps*ChR cDNA encoding the 7TM domain (amino acid residues 1–326) in frame with EYFP tag was generated as described previously (19). HEK293 (human embryonic kidney) cells were transfected using the TransPass COS/293 transfection reagent (New England Biolabs, Ipswich, MA). All-*trans*-retinal (Sigma) was added as a stock solution in ethanol at the final concentration of 5 μM. Measurements were performed 48–72 h after transfection with an Axopatch 200B amplifier (Molecular Devices) with a 2-kHz filter. The signals were digitized with a Digidata 1440A using the pClamp 10.2 software (both from Molecular Devices) at the sampling rate 50 μs/point for noise analysis and 200 μs/point for other experiments. Fabrication of patch pipettes and contents of pipette and bath solutions were as before (19). To test relative permeability for Na^+ ions, Na^+ in the bath solution was partially replaced with large monovalent cation *N*-methyl-D-glucamine that is not conducted by ChRs to a measurable degree (8). Light excitation was provided by a Polychrome IV light source (T.I.L.L. Photonics GMBH, Grafelfing, Germany) pulsed with a mechanical shutter (Uniblitz Model LS6; Vincent Associates, Rochester, NY; half-opening time, 0.5 ms). The light intensity was attenuated with the built-in Polychrome system or with neutral density filters. Maximal quantum density at the focal plane of the 40× objective lens was $\sim 2 \times 10^{22}$ photons $\times$ $m^{-2} \times s^{-1}$.

*Noise Analysis—*An experimental procedure for stationary noise analysis of ChR-generated whole cell currents was modified from Ref. 29. Current traces were recorded at −60 mV at room temperature in the dark and during a 25-s light pulse of intensity, eliciting a half-maximal response. The plateau current was fit with a single exponential, and the fit signal was subtracted from the current trace (30). Power spectral densities were calculated from 5-s segments of the traces using pClamp software; 10 individual spectra for dark and light conditions were averaged for each trace. The difference (light minus dark spectrum) was fit between 2 and 1 kHz with a single Lorentzian function to determine the zero frequency asymptote and the corner frequency (31).

The theory of stationary noise analysis is based on the assumption that the channel stochastically alternates between a closed and an open state (31). The spectral density of resultant current fluctuations is described by a Lorentzian function,

$$S(f) = \frac{S(0)}{1 + \left(\frac{f}{f_c}\right)^2} \qquad \text{(Eq. 1)}$$

where $S(f)$ is the spectral density, $S(0)$ is the zero asymptote (spectral density at 0 Hz), f is the frequency, and f_c is the corner frequency.

The unitary conductance (γ) is estimated from the parameters of this function using the amplitude of the whole cell channel current (I), the holding potential (V_h), and the reversal potential of the channel current (V_r).

$$\gamma = \frac{\pi S(0)\, f_c}{2I(V_h - V_r)} \qquad \text{(Eq. 2)}$$

Electrical Measurements in Neurons—The 7TM domains of *Ps*ChR or *Cr*ChR2 in frame with an EYFP tag were inserted into pFUGW lentivirus vector backbone provided by Dr. Carlos Lois (Massachusetts Institute of Technology) between BamHI and EcoRI sites. The lentivirus was produced by triple transfection of HEK293FT cells (Invitrogen) with the envelope plasmid pCMV-VSVG, the packaging plasmid pΔ8.9 (both from Dr. Lois), and the pFUGW-*Ps*ChR/*Cr*ChR2-EYFP plasmids using Lipofectamine 2000 (Invitrogen), as described (32). The viral titer was determined by infection of HEK cells. Hippocampi of embryonic day 18 Sprague-Dawley rats were obtained as part of a kit from BrainBits (Springfield, IL), and primary neuronal cultures were prepared using the protocol provided by the company. Cells were cultured in NbActiv4 medium (70) on poly-lysine-coated coverslips and supplemented with 0.4 μM all-*trans*-retinal (final concentration, in addition to retinyl acetate present in the medium), unless otherwise indicated. Neurons were infected with the lentivirus 1 day after plating. Between 10 and 19 days after plating, the cells were used for patch clamp measurements with the same setup as described for HEK cells, except that neurons were bathed in Tyrode's solution (125 mM NaCl, 2 mM KCl, 3 mM $CaCl_2$, 1 mM $MgCl_2$, 25 mM HEPES, 30 mM glucose, pH 7.3), and the pipette solution contained 135 mM KCl, 6 mM NaCl, 0.35 mM EGTA, 4 mM Mg-ATP, 20 mM HEPES, pH 7.25. Spiking was measured in the current clamp mode to keep the membrane voltage at approximately −65 mV.

Expression and Purification of PsChR in Pichia pastoris—The 7TM domain of *Ps*ChR with a TEV protease site at the N terminus, and a nine-His tag at the C terminus was subcloned into the pPIC9K vector (Invitrogen) via its EcoRI and AvrII sites. *P. pastoris* strain SMD1168 (*his4*, *pep4*) (Invitrogen) was transformed by electroporation using the linearized resultant plasmid pPIC9K-*Ps*ChR-9His. A *P. pastoris* clone that grows on 4 mg/ml Geneticin was selected according to the manufacturer's instructions. Protein expression and purification was carried out as described earlier for *Chlamydomonas augustae* channelrhodopsin 1 (33). Cells were grown in buffered glycerol-complex medium to A_{600} 2–6, transferred to buffered minimal methanol yeast medium supplemented with all-*trans*-retinal and induced with 0.5% methanol. After 24–30 h, the cells were harvested by low speed centrifugation and disrupted in a bead beater (BioSpec Products, Bartlesville, OK). The membranes were collected by ultracentrifugation and solubilized in 1.5% (w/v) dodecyl maltoside for 1 h at 4 °C. Nonsolubilized material was removed by ultracentrifugation, and protein was purified from the supernatant using a nickel-nitrilotriacetic acid column (Qiagen). The protein samples were concentrated in 100 mM NaCl, 0.02% dodecyl maltoside, 20 mM HEPES (pH 7.4) and used for measurements either directly or after reconstitution in nanodiscs with 1,2-dimyristoyl-*sn*-glycero-3-phosphocholine lipid from Avanti Polar Lipids (Alabaster, AL), as described for haloarchaeal sensory rhodopsin II in (34).

Absorption Spectroscopy and Flash Photolysis—Absorption spectra of partially purified *Ps*ChR in the UV-visible range were recorded on a Cary 4000 spectrophotometer (Varian, Palo Alto, CA). pH titration was carried out by the addition of small volumes of 1 M NaOH, 0.5 M Tris (pH 10), 0.5 M citric acid, or 1 M HCl. Light-induced absorption changes of *Pichia*-expressed

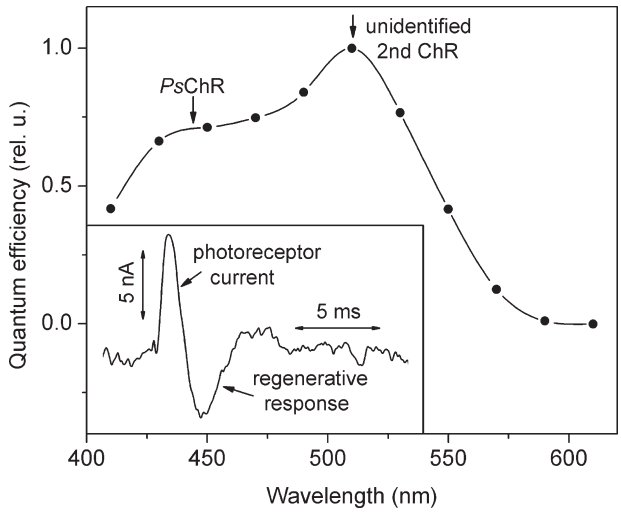

FIGURE 1. *Inset*, a typical photoinduced electrical signal recorded from a cell suspension of the marine alga *P. subcordiformis* consisting of a photoreceptor current followed by a regenerative response. *Main panel*, the action spectrum of photoreceptor currents in *P. subcordiformis*, which shows a contribution of two photoreceptor pigments. *rel. u.*, relative unit.

pigment were measured with a laboratory-constructed cross-beam apparatus (35). Excitation flashes (532 nm, 6 ns, 40 mJ) were provided by a Surelite I Nd-YAG laser (Continuum, Santa Clara, CA). Measuring light was from a 250-W incandescent tungsten lamp combined with a McPherson monochromator (model 272, Acton, MA). A Hamamatsu Photonics (Bridgewater, NJ) photomultiplier tube (model R928) was protected from excitation laser flashes by a second monochromator of the same type and additionally with 12-nm bandwidth interference filters (Oriel Instruments, Stratford, CT). Signals were amplified by a low noise current amplifier (model SR445A; Stanford Research Systems, Sunnyvale, CA) and digitized by a Digidata 1320A (Molecular Devices) at the sampling rate 4 μs/point. The time interval between excitation flashes was 10 s, and 100 sweeps were averaged for each data point.

Retinal Extraction and Analysis—The protocol was adapted from Refs. 36 and 37. Protein samples were kept overnight in the dark and maintained in darkness or illuminated for 2 min using a tungsten halogen light beam from an FOI-150W Illuminator (Titan Tool Supply, Buffalo, NY) passed through a heat filter and a 432 ± 5-nm interference filter. Retinal was extracted by the addition of ice-cold methanol followed by ice-cold hexane and vortexing under dim red light. Phases were separated by centrifugation, and the top layer (hexane phase) was carefully withdrawn and dried under argon. The samples were dissolved in methanol and separated in 100% hexane on a Spherisorb S5 ODS2 analytical column using a Waters Delta 600 HPLC system (Waters Corporation, Milford, MA).

Data analysis was performed with pClamp 10.2 (Molecular Devices) and OriginPro 7 (OriginLab Corporation, Northampton, MA) software.

RESULTS

Photoreceptor Currents in the Algae—Unilateral light excitation of suspensions of *P. subcordiformis* cells elicited characteristic photoelectric responses (Fig. 1, *inset*) previously detected in many freshwater flagellates (6, 38–40). They are comprised

of photoreceptor currents superimposed with the regenerative response triggered by depolarization of the plasma membrane. Gene silencing experiments in *C. reinhardtii* have demonstrated that photoreceptor currents are mediated by ChRs (4, 5, 41).

The action spectrum of photoreceptor currents in *P. subcordiformis* shows a main peak at 510 nm and a pronounced shoulder in the blue region (Fig. 1, *main panel*) that we attribute to the existence of two photoreceptor pigments, as demonstrated for the similar action spectrum in *C. reinhardtii* (4). Our data match closely the action spectrum of *P. subcordiformis* phototaxis determined by measuring accumulation of cells in an illuminated cuvette (42). Similar action spectra have also been measured in many other green flagellates, including the model organism *C. reinhardtii*, in which contribution of two ChRs to the phototaxis spectrum was directly proven by gene knockdown experiments (4). As we show below, the maximum of the spectral sensitivity of *Ps*ChR in HEK293 cells was at 445 nm, which strongly suggests it being one of the two receptors responsible for phototaxis in this organism. This hypothesis remains to be tested directly when methods for genetic modification of *P. subcordiformis* become available.

PsChR Primary Structure—The amino acid sequence of *Ps*ChR is comprised of 660 residues, and its N-terminal half forms the 7TM (rhodopsin) domain. Two more transmembrane helices are predicted in its C-terminal half, as in ChR1 from *C. reinhardtii*. Its N terminus (upstream of the 7TM domain) is relatively short and contains no predicted signal peptide, in contrast to *Cr*ChR1. Only Cys-73 (*Cr*ChR1 numbering) is conserved of three N-terminal Cys residues found to form disulfide bonds between protomers in the C1C2 dimer (43). *P. subcordiformis* is classified as a prasinophycean alga, but *Ps*ChR shows lower sequence homology with *Pg*ChR1 from another prasinophyte, *Pyramimonas gelidicola* (44), than with known ChRs from chlorophycean flagellates. It contains all five Glu residues and a Lys residue in helix B, conserved in ChRs from *C. reinhardtii* and *Volvox carteri* (supplemental Fig. S1). Glu and Asp residues are found, respectively, in the positions of the protonated Schiff base counterions Asp-85 and Asp-212 in bacteriorhodopsin (BR) and a His residue in the position of the proton donor Asp-96 in BR. Glu-87 of *Cr*ChR1, responsible for its pH-dependent color tuning and fast photocurrent inactivation (45), is also conserved in *Ps*ChR. The position of Tyr-226/Asn-187 (in *Cr*ChR1/*Cr*ChR2, respectively), identified as one of the molecular determinants of differences in spectra, desensitization, and current kinetics in response to a step-up and step-down of continuous light between *Cr*ChR1 and *Cr*ChR2 (46), in *Ps*ChR is occupied by a Ser residue.

Kinetics and Inactivation of PsChR Currents—The 7TM domain of *Ps*ChR expressed in HEK293 cells demonstrated light-gated channel activity typical of other high efficiency ChRs (Fig. 2). The mean peak current generated by *Ps*ChR at saturating light intensity was 4.6 ± 0.4 nA (n = 27 cells), compared with 2.5 ± 0.2 nA (n = 20 cells) for *Cr*ChR2, the channelrhodopsin most frequently used in optogenetic studies (Fig. 2*C*). The difference between the plateau currents for these two pigments was even greater: ~3-fold (Fig. 2*C*). Under continuous illumination, the photocurrent decreased from a peak to a

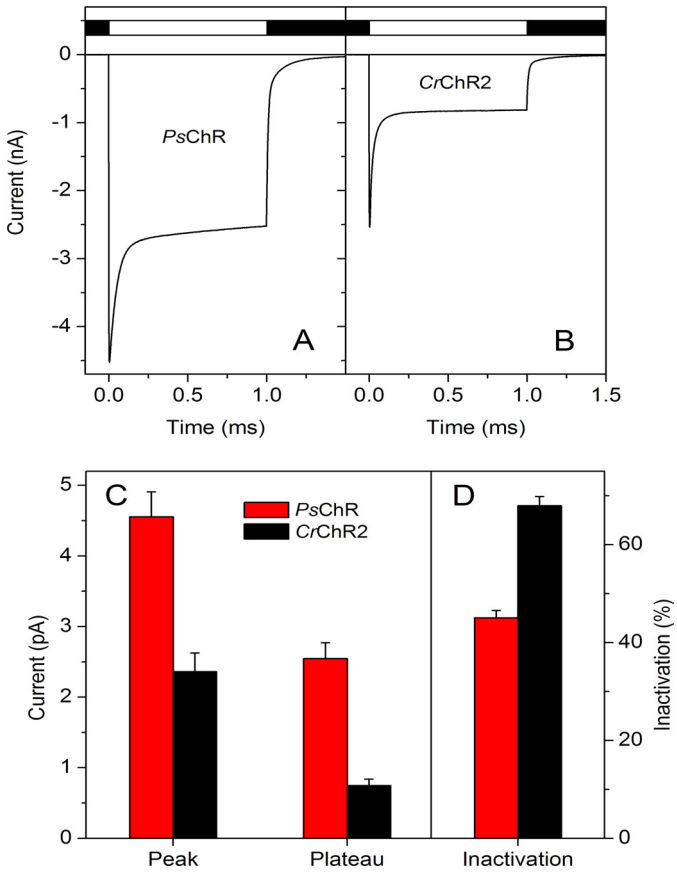

FIGURE 2. *A* and *B*, photocurrents generated by *Ps*ChR (*A*) and *Cr*ChR2 (*B*) expressed in HEK293 cells in response to a light pulse of saturating intensity (440 and 470 nm, respectively). The duration of the pulse is shown schematically on top. *C* and *D*, the mean amplitudes of peak and plateau currents (*C*) and the degree of current inactivation (*D*) for *Ps*ChR (n = 27 cells) and *Cr*ChR2 (n = 20 cells).

quasistationary level, which is also known for all other ChRs and is called light inactivation or desensitization. For *Ps*ChR the rate of this process was slower, and its extent was significantly less than that of *Cr*ChR2 (Fig. 2). In addition to the main phase of inactivation with the time constant (τ) ~40 ms, which contributed 76% of the amplitude, a slow second phase with τ ~7 s was observed (saturating light intensity, −60 mV, pH 7.4). Current inactivation after 1-s illumination, calculated as the difference between the peak and plateau current relative to the peak current, was ~1.5-fold less for *Ps*ChR than for *Cr*ChR2 (Fig. 2*D*). After switching off the light, *Ps*ChR currents decayed biexponentially with τ of both phases ~15% larger (τ_1 = 9.8 ± 0.3 ms, τ_2 = 102 ± 5.4 ms, n = 24 cells) than those for *Cr*ChR2 currents under the same conditions (τ_1 = 8.3 ± 0.6 ms, τ_2 = 84.9 ± 11.3 ms, n = 16 cells).

Current Amplitude and Unitary Conductance—The amplitude of the whole cell current measured under continuous illumination depends on the number of photoactive molecules in the cell membrane, lifetime of the open channel, and its unitary conductance. Although single channel currents generated by *Cr*ChR2 are below the limit for direct recording, their parameters could be estimated by stationary noise analysis (29). We used this approach (for details see "Experimental Procedures") to determine whether a greater plateau current of *Ps*ChR reflects an increased unitary conductance over that of *Cr*ChR2.

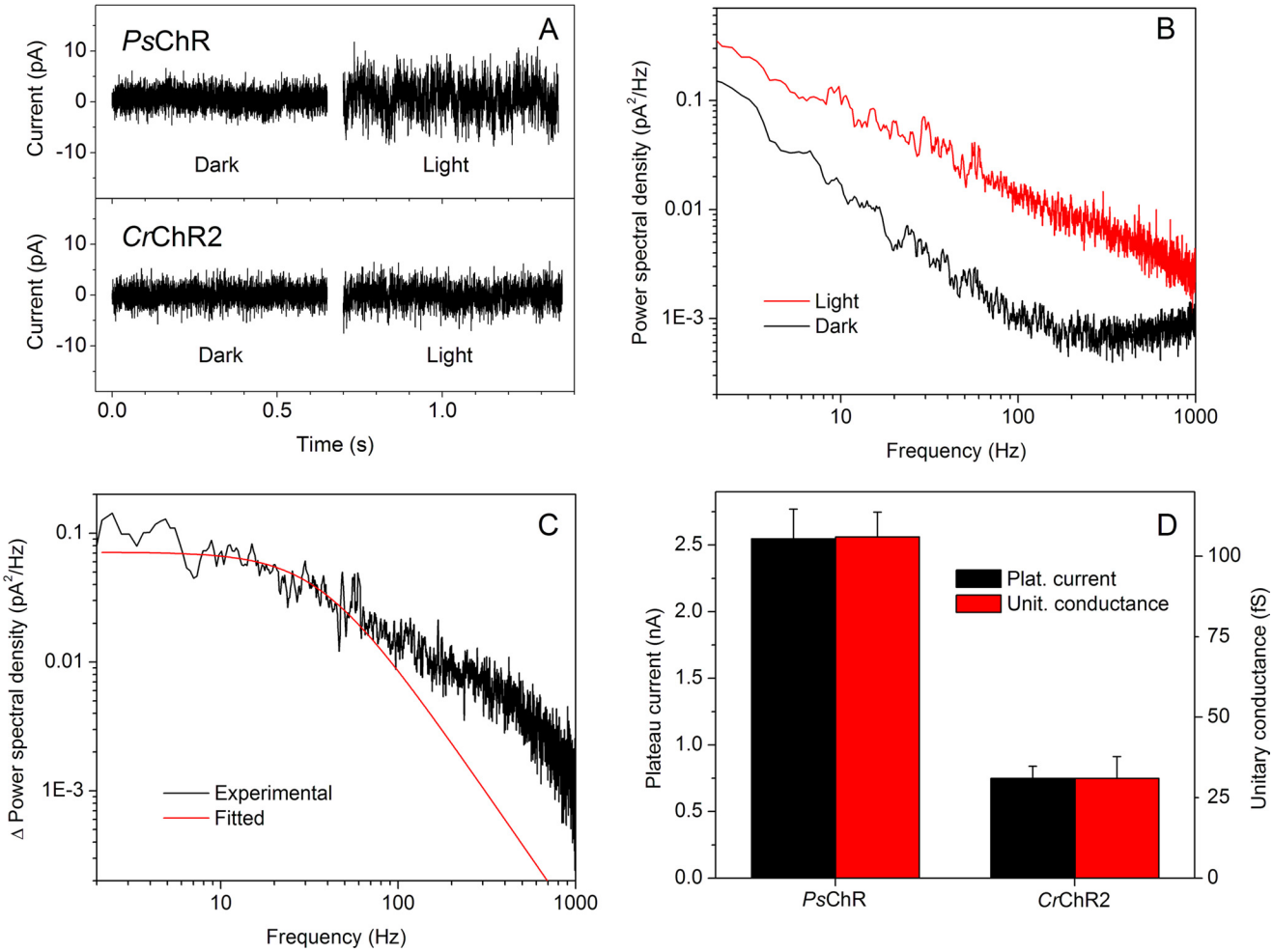

FIGURE 3. *A*, whole cell current noise generated by *Ps*ChR (*top*) and *Cr*ChR2 (*bottom*) in the dark and under continuous illumination. *B*, noise power spectra calculated for the dark (*black line*) and light (*red line*) conditions of currents generated by *Ps*ChR. The spectra were smoothed by five-point adjacent averaging for presentation purposes. Other details are under "Experimental Procedures." *C*, the difference spectrum (light minus dark) calculated from the spectra shown in *B* (*black line*) and its single Lorentzian fit (*red line*). *D*, plateau currents measured after 1-s illumination (*left axis*; same as in Fig. 2*C*) and unitary conductances (*right axis*) of *Ps*ChR and *Cr*ChR2. The data are the mean values calculated from 12 individual current traces for *Ps*ChR and 8 traces for *Cr*ChR2.

In *Ps*ChR-transfected cells, the noise amplitude became considerably larger under continuous illumination, as compared with the dark conditions (Fig. 3*A*, *top traces*). This increase in noise was much greater than observed in *Cr*ChR2-transfected cells under the same conditions (Fig. 3*A*, *bottom traces*). The noise of control untransfected cells did not change at all after switching on the light (data not shown). The power density spectra for both light and dark conditions contained a significant $1/f$ component, *i.e.*, a component inversely proportional to the frequency (Fig. 3*B*). The origin of this noise component is unclear; it can arise simply from nonstationary processes such as base-line drift (30) or from the summation of a few Lorentzian components having appropriate amplitudes and corner frequencies (47). However, the light minus dark difference could be fit with a Lorentzian function between 2 and 1 kHz (Fig. 3*C*). The value of unitary conductance (γ) for *Ps*ChR obtained from this fit was ~3-fold larger than for *Cr*ChR2. Our value for *Cr*ChR2 was close to that reported previously (29), taking into account the lower bath Na^+ concentration in our experiments and the temperature dependence of γ. The close correlation between the whole cell plateau current amplitudes and the calculated unitary conductances (Fig. 3*D*) shows that the greater current amplitude of *Ps*ChR in HEK cells over that of *Cr*ChR2 is attributable to its greater unitary conductance. It should be noted that the absolute values of γ for both pigments determined by this method may be underestimated, because the plateau current generated by ChRs under prolonged illumination is largely determined by a third, inactivated state of the channel (8), not taken into account by the model used.

Current Peak Recovery—A general property of all ChRs tested so far is that a second light pulse delivered after a short dark interval elicits a response with a smaller transient peak than that invoked by the first pulse, although the plateau level is the same for both pulses (Fig. 4*A*). The time course of this process is multicomponential and depends on the membrane potential and extracellular pH (8). The recovery of the peak current generated by *Ps*ChR was faster than that of any ChR tested so far. In particular, 50% of the initial peak amplitude was recovered in a ~30-fold shorter time than with *Cr*ChR2 measured under the same conditions (Fig. 4*B*).

Ion Selectivity—Inward photocurrents generated by *Ps*ChR under our standard conditions were almost entirely carried by

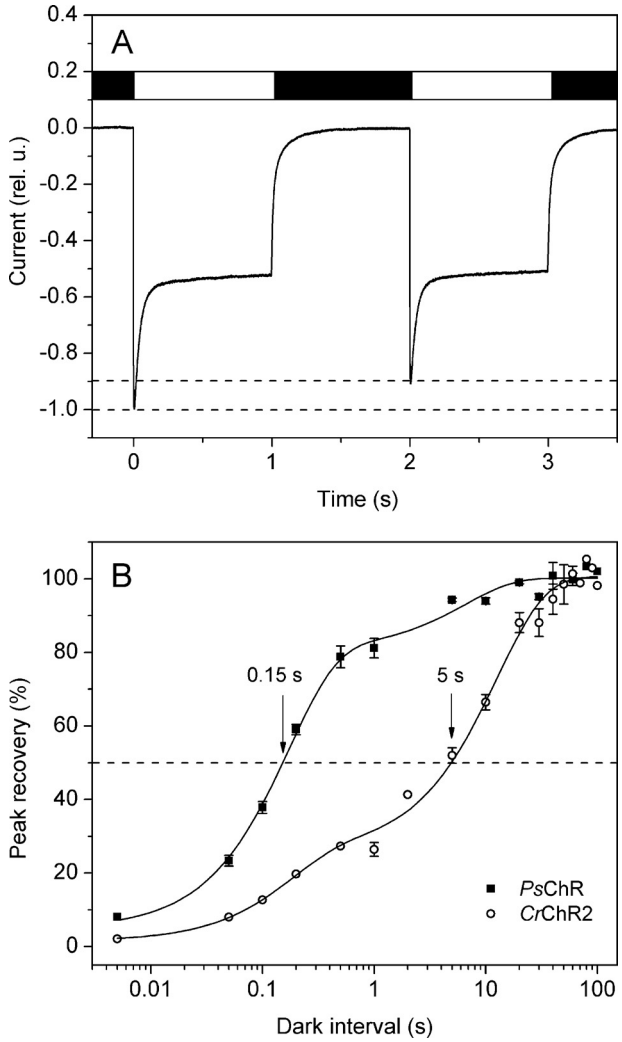

FIGURE 4. *A*, photocurrents generated by *Ps*ChR expressed in an HEK293 cell in response to a pair of 1-s light pulses (440 nm, saturating intensity) delivered with a 1-s dark interval. Current was normalized to the peak value of the first signal. The illumination protocol is shown schematically on top. *B*, the time course of the recovery of the transient component of the signal measured with *Ps*ChR (*black squares*) or *Cr*ChR2 (*open circles*). Recovery was calculated as the ratio of the differences between the peak and the plateau values measured in response to the second and the first pulse. Recovery percentage is plotted against the time interval between the pulses. The data are the mean values of measurements in three to five cells.

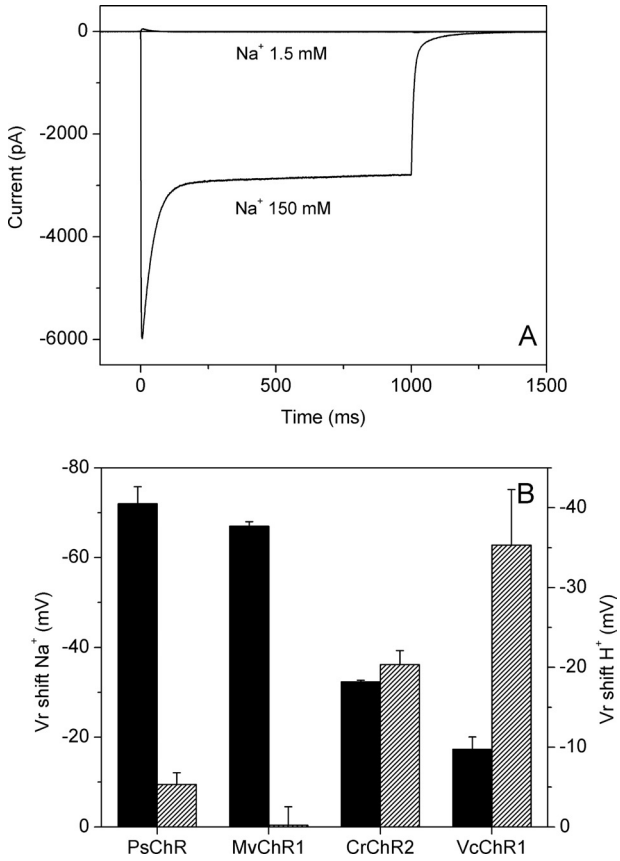

FIGURE 5. *A*, photocurrents generated by *Ps*ChR in the same HEK293 cell at 150 and at 1.5 mM Na^+ and 148.5 mM nonpermeable *N*-methyl-D-glucamine in the bath (1-s light stimulus, 440 nm). *B*, shifts of V_r measured for plateau currents after a decrease in the bath Na^+ concentration from 150 to 1.5 mM (*left axis*, *solid bars*), or an increase in the bath pH from 7.4 to 9 (*right axis*, *hatched bars*). The data points are the mean values obtained from three cells.

Na^+ ions, as revealed by their dramatic suppression after partial replacement of Na^+ in the bath with nonpermeable organic *N*-methyl-D-glucamine (Fig. 5*A*). In comparison, only ~80% of *Cr*ChR2 current was contributed by Na^+, as estimated in a parallel experiment (data not shown; see Refs. 8 and 45). We measured the current-voltage relationships and calculated the shifts of the reversal voltage (V_r) upon a decrease of Na^+ or H^+ concentrations in the bath for *Ps*ChR and several other ChRs for comparison. The greatest negative shifts upon Na^+ depletion were obtained with *Ps*ChR and *Mv*ChR1 from *Mesostigma viride*, which indicated their highest relative permeability to Na^+ ions over protons of all tested ChRs (Fig. 5*B*). However, the Na^+ conductance of *Mv*ChR1 was inhibited by protons; peak current amplitude decreased 24% when the bath pH was changed from 7.4 to 6.4, despite a ~7-mV positive shift of the V_r, indicating that protons were also permeable through its channel. In contrast, no such inhibition was observed in *Ps*ChR: the current amplitude difference between pH 7.4 and 6.4 was <2%.

Under our conditions, the V_r of *Cr*ChR2 current shifted to a less positive value during illumination (from 15.8 ± 1.0 mV for the initial current to 10.7 ± 1.2 mV for the plateau current; n = 6 cells). These observations confirmed the previously reported data interpreted as the presence of two open states with different ion selectivities in the photocycle of this pigment (48). In contrast, the corresponding V_r values calculated for *Ps*ChR current were approximately the same (13.1 ± 0.6 mV and 14.1 ± 0.6 mV, respectively; n = 7 cells). According to the above interpretation, *Ps*ChR appears to exhibit a single conductive state, in contrast to *Cr*ChR2.

Action Spectroscopy—The action spectra of *Ps*ChR-generated currents were measured using a 50-ms light pulse of low intensity, as described earlier for *Mv*ChR1 (40). Its maximum was at 445 nm (Fig. 6*A*, *black line*), which makes *Ps*ChR the shortest wavelength-absorbing ChR so far characterized.

Interaction of the protonated Schiff base and its counterion is one of the major mechanisms of spectral tuning in retinylidene proteins (49). Most ChRs (except *Ds*ChR1) contain two carboxylate residues homologous to Asp-85 and Asp-212 in BR (supplemental Fig. S1) that form hydrogen bonds with the Schiff base nitrogen, as revealed by the crystal structure of the C1C2

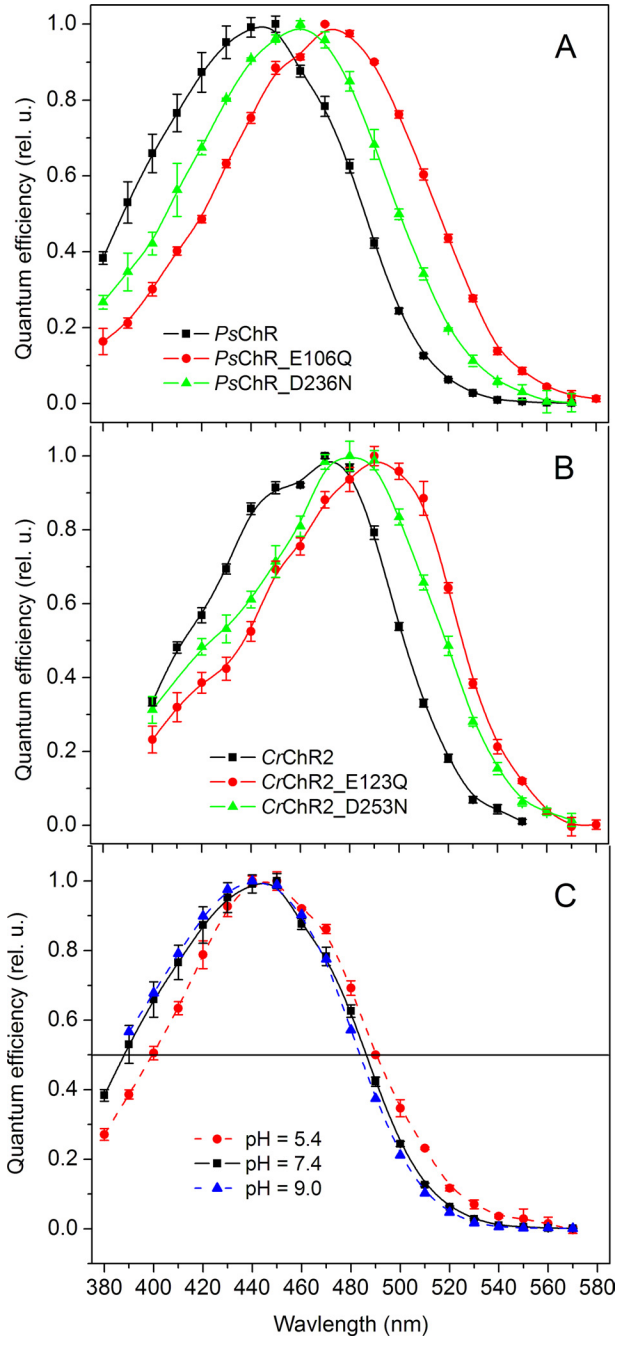

FIGURE 6. **Action spectra of channel currents generated in HEK293 cells by wild-type *Ps*ChR and its mutants at the bath pH 7.4 (*A*), wild-type *Cr*ChR2 and its mutants at the bath pH 7.4 (*B*), and wild-type *Ps*ChR at the bath pH indicated in the legend (*C*).** The data points are the mean values of three to five measurements. *rel. u.*, relative unit.

chimera (43). We generated the E106Q and D236N mutants to neutralize each of the corresponding carboxylate positions in *Ps*ChR and measured their spectral sensitivities. Both mutations caused a red shift of the spectrum (Fig. 6*A*), the magnitude of which was larger upon neutralization of the Asp-85 homolog (30 nm) than of the Asp-212 homolog (14 nm), as is seen in BR (50–52). Similar results (red shifts of 23 and 16 nm) were found in the corresponding *Cr*ChR2 mutants, E123Q and D253N (Fig. 6*B*), the first of which was previously tested in oocytes (53). This is in contrast to low efficiency *C. augustae* channelrhodopsin 1, in which the corresponding mutations caused a blue spectral shift,[3] as did threonine substitution of the Asp-85 homolog in the C1V1 chimera (17). The opposite directions of the spectral shifts suggest different counterion arrangements in these ChRs.

Acidification of the medium also caused a red shift of the *Ps*ChR action spectrum, but its magnitude was relatively smaller compared with those observed in the counterion mutants: less than 3 nm when pH was shifted from 9.0 to 7.4 and 4 nm when pH was shifted from 7.4 to 5.4 (Fig. 6*C*). This observation may indicate low pK_a values of the titrated carboxylates. However, taking into account that channel activity of the E106Q and D236N mutants was greatly reduced (~44- and ~100-fold, respectively, with respect to that of wild type), an alternative explanation could be smaller contributions of the protonated red-shifted forms of the pigment to the net photocurrents compared with that of the unprotonated forms.

*Characterization of Purified PsChR—Ps*ChR was expressed in *P. pastoris* and partially purified in detergent with yields of 0.2–0.3 mg/liter of yeast culture. The absorption spectrum of purified *Ps*ChR in dodecyl maltoside showed an absorption maximum at 437- and ~90-nm half-bandwidth (Fig. 7*A*, *solid line*). The absorption spectrum shifted less than 1–2 nm to longer wavelengths when pigment molecules were incorporated into lipid nanodiscs (Fig. 7*A*, *dashed line*). Both spectra lacked obvious vibrational fine structure, characteristic of the other relatively blue-shifted microbial rhodopsins *Cr*ChR2 (54, 55) and haloarchaeal sensory rhodopsin II (56).

The absorption spectrum of purified *Ps*ChR also shifted to longer wavelengths upon acidification of the medium, as did the action spectrum of channel currents. Interestingly, the maximum at 445 nm (the peak of the action spectrum) was observed at the nonphysiological pH ~4.3, which suggests different protein states in detergent and biological membranes (Fig. 7*B*). Titration of the peak revealed at least three titratable groups. The shape of the differential signal for the most alkaline transition (data not shown) indicated that it reflects deprotonation of the Schiff base; hence fitting of the titration data was performed with the base level parameter fixed at 360 nm. The pK_a of this transition was ~10.5, and those of the other two transitions were 3.8 and 6.6. It is probable that the most acidic transition reflects protonation of Glu-106, because neutralization of this residue caused a larger red shift of the action spectra of the two mutants tested (Fig. 6*A*, *red line*). The transition with pK_a ~6.6 and smaller amplitude may correspond to protonation of Asp-236, a neutral mutation of which caused a smaller red spectral shift (Fig. 6*A*, *green line*). This hypothesis needs to be tested with purified mutant proteins, which are, however, not yet available.

Retinal extraction experiments showed that the ratio of all-*trans*- to 13-*cis*-isomer in dark-adapted *Ps*ChR was ~75:25, similar to that in *Cr*ChR2 (37). No significant changes in the isomer composition were observed upon light adaptation. In BR and *Anabaena* sensory rhodopsin, changes in the isomer composition (36, 57) upon dark adaptation give rise to characteristic difference spectra (36, 58). The direction of the

[3] E. G. Govorunova, O. A. Sineshchekov, H. Li, and J. L. Spudich, manuscript in preparation.

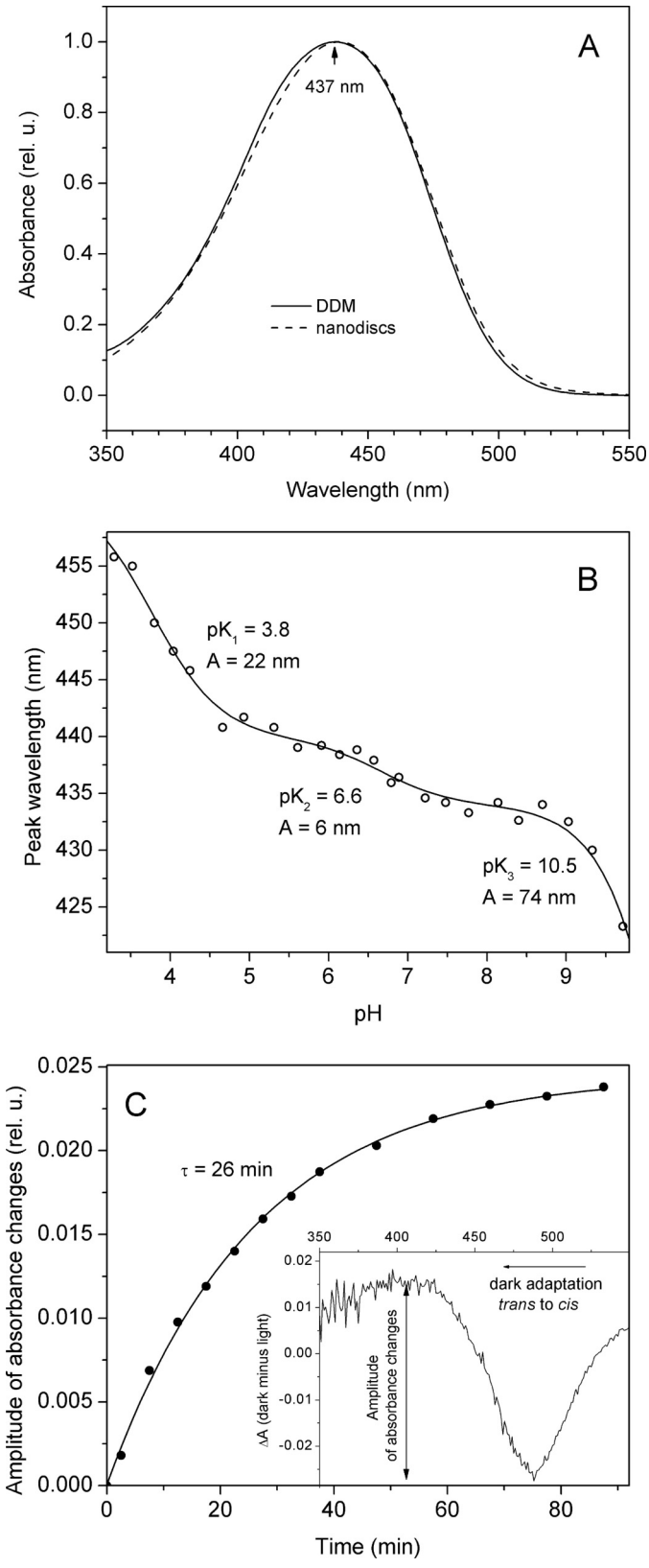

FIGURE 7. *A*, the absorption spectrum of purified *Ps*ChR solubilized in detergent or reconstituted in nanodiscs. *B*, pH titration of the absorption maximum of detergent-purified *Ps*ChR. Experimental data were fit with a sum of three Henderson-Hasselbalch components ($f(\mathrm{pH}) = A \times (1 - 10^{(\mathrm{pH}-\mathrm{pK}_a)})^{-1} + C$). The pK values and amplitudes of the transitions denoted by *A* are derived from curve fitting. *C*, *inset*, the difference spectrum between dark- and light-adapted purified *Ps*ChR. *Main panel*, the time course of the spectral transition during dark adaptation determined as the dependence of the amplitude of the difference spectrum (as shown by the *arrow* in the *inset*) on time fit with an exponential function. *rel. u.*, relative unit.

observed changes are opposite in BR and *Anabaena* sensory rhodopsin. We carried out spectroscopic measurements to resolve possible small amplitude changes in *Ps*ChR that fall below the detection limit of retinal extraction and to follow their time course. Dark adaptation of *Ps*ChR led to a blue spectral shift with a typical light-dark adaptation shape of the difference spectrum (Fig. 7*C*, *inset*). As in BR, the amount of 13-*cis*-retinal increased in the dark. However, its magnitude in *Ps*ChR was dramatically smaller as judged from the difference spectrum (only 3% of the total absorbance). The time constant of dark adaptation in *Ps*ChR was ~26 min (Fig. 7*C*, *main panel*).

Fig. 8*A* shows the spectra of laser flash-induced absorbance changes in detergent-purified *Ps*ChR. Although no positive signal was observed in the short wavelength region at room temperature, an increase in the absorption at 510 nm at the expense of a decrease at 380 nm at the early stages of the photocycle suggests contribution of an early M-like state, the absorption of which strongly overlaps with the absorption of the unphotolysed state. Therefore, kinetics of this intermediate was followed at 5 °C to improve the time resolution (Fig. 8*B*). Even at this low temperature, the rates of the M intermediate formation and decay were faster than those reported in *Cr*ChR2 (59). Consequently, maximal accumulation of the M intermediate of *Ps*ChR was observed at 50 μs, as compared with 200 μs in *Cr*ChR2. The main photoproduct (N/O-like) in the *Ps*ChR photocycle is red-shifted, similar to observations in *Cr*ChR2 (54), and biphasic in both its rise and decay. The rise and the fast component of the decay roughly correlated with the opening and closing of the channel measured in HEK cells (Fig. 8*C*).

Function of PsChR in Neurons—To test whether *Ps*ChR is relevant for optogenetic applications, we examined its performance in cultured hippocampal neurons. Neurons expressing *Ps*ChR were capable of firing action potentials upon light stimulation with brief light pulses at frequencies up to 50 Hz (Fig. 9*A*), which is the upper limit for pyramidal neurons (20). Expression of both *Ps*ChR and *Cr*ChR2, as judged by the tag fluorescence, was increased when the cultures were supplemented with all-*trans*-retinal (final concentration, 0.4 μM) in addition to 0.5 μM retinyl acetate present in the culture medium. Photoinduced channel currents generated in neurons by *Ps*ChR were increased ~9-fold, and those generated by *Cr*ChR2 were increased ~5-fold in cultures with additional retinal, which was similar to results obtained in HEK293 cells (~12- and ~2.4-fold increase for *Ps*ChR and *Cr*ChR2, respectively).

Upon 1-Hz excitation, the rate of the membrane depolarization decreased significantly more slowly and to a lesser degree for *Ps*ChR than for *Cr*ChR2 (Fig. 9, *B* and *C*, *left axes*). Correspondingly, the probability of spike generation driven by this depolarization only slightly decreased during a 20-s period of excitation in *Ps*ChR-expressing neurons, whereas in *Cr*ChR2-expressing neurons it rapidly dropped to a much lower level (Fig. 9, *B* and *C*, *bars*, *right axes*).

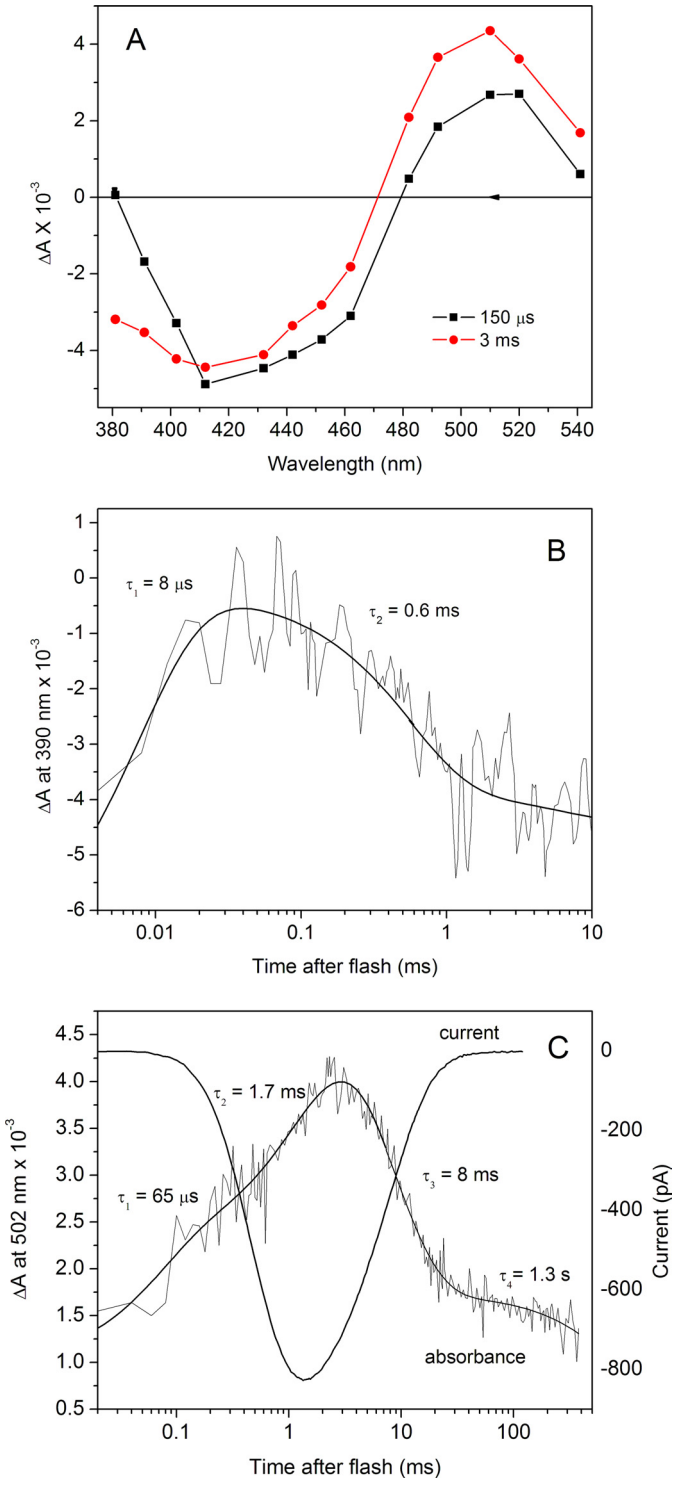

FIGURE 8. *A*, the spectra of absorbance changes induced by laser excitation (532 nm, 6 ns) in detergent-purified *Ps*ChR. *B*, the kinetics of the M-like intermediate in detergent-purified *Ps*ChR. The *smooth line* shows a computer fit to the data. *C*, superposition of the kinetics of the red-shifted intermediate in the photocycle of detergent-purified *Ps*ChR and the kinetics of the laser flash-induced photocurrent generated by *Ps*ChR in a HEK293 cell adapted from Ref. 19.

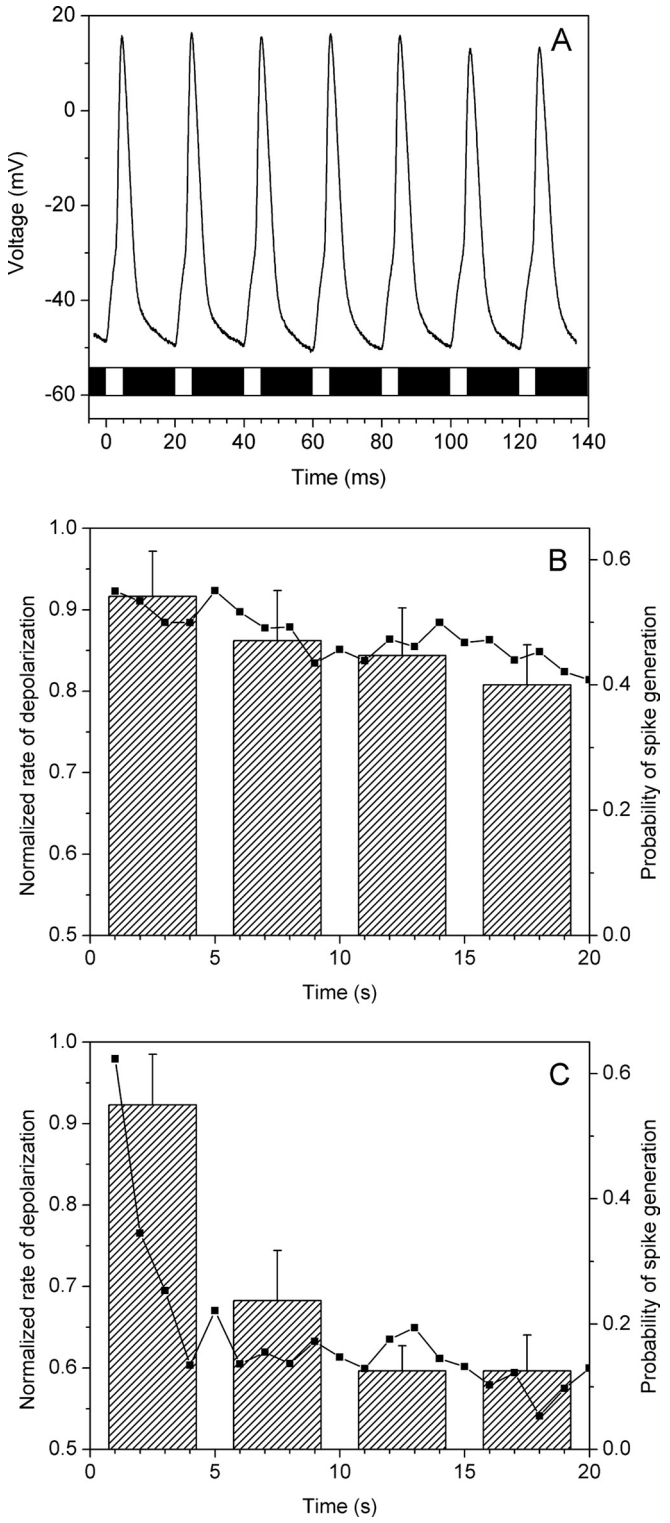

FIGURE 9. *A*, typical voltage traces showing membrane depolarization and spikes recorded from a current-clamped *Ps*ChR-expressing pyramidal neuron in response to stimulation with brief light pulses (440 nm, 5 ms, 50 Hz). The times of light pulses are indicated by the *bar* at the *bottom* of the graph. *B* and *C*, the normalized rate of the light-induced membrane depolarization (*squares*, *left axis*) and the probability of spike generation (*bars*, *right axis*) in cultured hippocampal neurons that express *Ps*ChR (*B*) or *Cr*ChR2 (*C*). Trains of 20 light pulses (5-ms duration) were applied at a frequency of 1 Hz. The excitation wavelength was 440 nm for *Ps*ChR and 470 nm for *Cr*ChR2, and the light intensity was close to the threshold for spike generation (*i.e.*, spikes were evoked by less than 100% of pulses). The spiking probability was calculated for each successive group of five pulses. The data are mean values recorded from 16 experiments.

DISCUSSION

Action spectroscopy and analysis of photoreceptor currents predict the existence of two spectrally distinct ChRs in all green algae tested so far (for review see Ref. 1), with a possible excep-

tion of *M. viride* (40). In *C. reinhardtii*, gene silencing experiments have directly confirmed the role of its ChRs as light receptors for phototaxis and the photophobic response (4, 5, 41). To date, two channelopsin genes per genome have been identified in *C. reinhardtii* (4, 7, 8, 60), *V. carteri* (61), and *Pleudorina starrii* (44). ChRs from *C. reinhardtii* and *V. carteri* have been heterologously overexpressed and purified, and their absorption spectra confirmed the results of action spectroscopy (41, 54, 61). In both organisms, the longer wavelength (green) absorbing ChR of the pair was designated as ChR1, and the shorter wavelength (blue) absorbing as ChR2.

Alignment of the 14 currently reported ChR sequences (supplemental Fig. S1) do not divide them in two distinct groups. Therefore, when only one ChR species of a presumed pair is known in a particular organism, it is difficult to assign it to ChR group 1 or 2 from the sequence information alone. (These numbers are not to be confused with type 1 and type 2 used to distinguish microbial rhodopsins from animal visual proteins (62).) However, matching the spectral properties of *Ps*ChR with the action spectrum of photoreceptor currents in *P. subcordiformis* clearly indicates that it is the blue-shifted member of the pair and consequently can be classified as *Ps*ChR2, despite it being the only ChR identified so far in this alga. *Ps*ChR absorption is the most blue-shifted of all known ChRs. Generally, for optogenetic tools long-wavelength absorption is preferable to minimize scattering of light by biological tissues and its absorption by hemoglobin. However, the blue-shifted spectrum of *Ps*ChR is ideal for combinatorial applications with long wavelength-absorbing rhodopsin pumps or fluorescent indicators.

All known ChRs are predominantly proton channels, so their use for optogenetics may lead to undesirable acidification of the cytoplasm. Indeed, a pH decrease of 0.3 units was detected in photoactivated HEK293 cells that express *Cr*ChR2 (15). The higher selectivity of *Ps*ChR for Na^+ ions over protons may circumvent this side effect. Both *Ps*ChR and *Mv*ChR1 show high Na^+ selectivity, but its mechanisms appear to be fundamentally different in these proteins. In *Mv*ChR1, which uniquely contains an alanine residue in place of His-134 (*Cr*ChR2 numbering), Na^+ conductance is inhibited by protons, as it is in the H134(R/S) mutants of *Cr*ChR2 (63). On the other hand, no such inhibition was found in *Ps*ChR, in which His-134 is conserved (supplemental Fig. S1).

Also conserved in *Ps*ChR are Glu-90, Ser-63, and Asn-258 (supplemental Fig. S1), implicated in control of ion selectivity in *Cr*ChR2 (63–65), and Ser-136, which regulates the size of the channel pore (66). Of three positively charged residues that form a vestibule on the extracellular side of the channel pore in C1C2 (43), Lys-154 is substituted with Val in *Ps*ChR. However, neutral residues are also found in this position in other ChRs, including highly proton-selective *Ds*ChR1, which is inconsistent with a possible role for this residue in determination of Na^+ selectivity. The structural determinants of the high Na^+ selectivity in *Ps*ChR remain currently unknown.

We showed that *Ps*ChR is expressed in cultured hippocampal neurons and can be used to drive their spiking activity by light excitation. Moreover, a faster peak recovery of *Ps*ChR-generated currents provides an advantage in certain optogenetic applications. Recently it has been demonstrated that the level of expression and, correspondingly, the amplitude of channel currents generated by *Cr*ChR2 in animal cells dramatically increase upon the addition of exogenous retinal (67). We found that this increase was even larger for *Ps*ChR than for *Cr*ChR2. Retinal content of some heterologous systems, such as *Caenorhabditis elegans* or *Drosophila*, is so low that even *Cr*ChR2 cannot be used there without the addition of exogenous retinal (68, 69). On the other hand, the intact mammalian brain may have enough endogenous retinal to reconstitute fully functional *Ps*ChR.

Our characterization of *Ps*ChR augments understanding of functional mechanisms of ChRs and reveals its potentially useful properties as an optogenetic tool. Taking into account the great number and diversity of phototactic algal species in which the existence of ChRs is predicted, comparative analysis of different native ChR variants may be as beneficial as bioengineering of select model molecules both for basic research into their structure-function relationships and for optimization of their biotechnology applications.

Acknowledgment—We thank Dr. Carlos Lois (Massachusetts Institute of Technology) for pFUGW, pCMV-VSVG, and pΔ8.9 plasmids.

REFERENCES

1. Sineshchekov, O. A., and Spudich, J. L. (2005) Sensory rhodopsin signaling in green flagellate algae, in *Handbook of Photosensory Receptors*, pp. 25–42, Wiley-VCH, Weinheim
2. Hegemann, P. (2008) Algal sensory photoreceptors. *Annu. Rev. Plant. Biol.* **59,** 167–189
3. Litvin, F. F., Sineshchekov, O. A., and Sineshchekov, V. A. (1978) Photoreceptor electric potential in the phototaxis of the alga *Haematococcus pluvialis*. *Nature* **271,** 476–478
4. Sineshchekov, O. A., Jung, K.-H., and Spudich, J. L. (2002) Two rhodopsins mediate phototaxis to low- and high-intensity light in *Chlamydomonas reinhardtii*. *Proc. Natl. Acad. Sci. U.S.A.* **99,** 8689–8694
5. Govorunova, E. G., Jung, K.-W., Sineshchekov, O. A., and Spudich, J. L. (2004) *Chlamydomonas* sensory rhodopsins A and B. Cellular content and role in photophobic responses. *Biophys. J.* **86,** 2342–2349
6. Sineshchekov, O. A., Govorunova, E. G., Der, A., Keszthelyi, L., and Nultsch, W. (1992) Photoelectric responses in phototactic flagellated algae measured in cell suspension. *J. Photochem. Photobiol. B Biol.* **13,** 119–134
7. Nagel, G., Ollig, D., Fuhrmann, M., Kateriya, S., Musti, A. M., Bamberg, E., and Hegemann, P. (2002) Channelrhodopsin-1. A light-gated proton channel in green algae. *Science* **296,** 2395–2398
8. Nagel, G., Szellas, T., Huhn, W., Kateriya, S., Adeishvili, N., Berthold, P., Ollig, D., Hegemann, P., and Bamberg, E. (2003) Channelrhodopsin-2, a directly light-gated cation-selective membrane channel. *Proc. Natl. Acad. Sci. U.S.A.* **100,** 13940–13945
9. Deisseroth, K. (2011) Optogenetics. *Nat. Methods* **8,** 26–29
10. Mei, Y., and Zhang, F. (2012) Molecular tools and approaches for optogenetics. *Biol. Psychiatry* **71,** 1033–1038
11. Hegemann, P., and Nagel, G. (2013) From channelrhodopsins to optogenetics. *EMBO Mol. Med.* **5,** 171–176
12. Yawo, H., Asano, T., Sakai, S., and Ishizuka, T. (2013) Optogenetic manipulation of neural and non-neural functions. *Dev. Growth Differ.* **55,** 474–490
13. Hegemann, P., and Möglich, A. (2011) Channelrhodopsin engineering and exploration of new optogenetic tools. *Nat. Methods* **8,** 39–42
14. Mattis, J., Tye, K. M., Ferenczi, E. A., Ramakrishnan, C., O'Shea, D. J., Prakash, R., Gunaydin, L. A., Hyun, M., Fenno, L. E., Gradinaru, V., Yizhar, O., and Deisseroth, K. (2012) Principles for applying optogenetic tools derived from direct comparative analysis of microbial opsins. *Nat. Meth-*

ods **9,** 159–172
15. Lin, J. Y., Lin, M. Z., Steinbach, P., and Tsien, R. Y. (2009) Characterization of engineered channelrhodopsin variants with improved properties and kinetics. *Biophys. J.* **96,** 1803–1814
16. Berndt, A., Schoenenberger, P., Mattis, J., Tye, K. M., Deisseroth, K., Hegemann, P., and Oertner, T. G. (2011) High-efficiency channelrhodopsins for fast neuronal stimulation at low light levels. *Proc. Natl. Acad. Sci. U.S.A.* **108,** 7595–7600
17. Yizhar, O., Fenno, L. E., Prigge, M., Schneider, F., Davidson, T. J., O'Shea, D. J., Sohal, V. S., Goshen, I., Finkelstein, J., Paz, J. T., Stehfest, K., Fudim, R., Ramakrishnan, C., Huguenard, J. R., Hegemann, P., and Deisseroth, K. (2011) Neocortical excitation/inhibition balance in information processing and social dysfunction. *Nature* **477,** 171–178
18. Prigge, M., Schneider, F., Tsunoda, S. P., Shilyansky, C., Wietek, J., Deisseroth, K., and Hegemann, P. (2012) Color-tuned channelrhodopsins for multiwavelength optogenetics. *J. Biol. Chem.* **287,** 31804–31812
19. Sineshchekov, O. A., Govorunova, E. G., Wang, J., Li, H., and Spudich, J. L. (2013) Intramolecular proton transfer in channelrhodopsins. *Biophys. J.* **104,** 807–817
20. Zhang, F., Prigge, M., Beyrière, F., Tsunoda, S. P., Mattis, J., Yizhar, O., Hegemann, P., and Deisseroth, K. (2008) Red-shifted optogenetic excitation. A tool for fast neural control derived from *Volvox carteri*. *Nat. Neurosci.* **11,** 631–633
21. Han, X., Qian, X., Stern, P., Chuong, A. S., and Boyden, E. S. (2009) Informational lesions. Optical perturbation of spike timing and neural synchrony via microbial opsin gene fusions. *Front. Mol. Neurosci.* **2,** 12
22. Tang, W., Ehrlich, I., Wolff, S. B., Michalski, A. M., Wölfl, S., Hasan, M. T., Lüthi, A., and Sprengel, R. (2009) Faithful expression of multiple proteins via 2A-peptide self-processing. A versatile and reliable method for manipulating brain circuits. *J. Neurosci.* **29,** 8621–8629
23. Kleinlogel, S., Terpitz, U., Legrum, B., Gökbuget, D., Boyden, E. S., Bamann, C., Wood, P. G., and Bamberg, E. (2011) A gene-fusion strategy for stoichiometric and co-localized expression of light-gated membrane proteins. *Nat. Methods* **8,** 1083–1088
24. Tsuda, S., Kee, M. Z., Cunha, C., Kim, J., Yan, P., Loew, L. M., and Augustine, G. J. (2013) Probing the function of neuronal populations. Combining micromirror-based optogenetic photostimulation with voltage-sensitive dye imaging. *Neurosci. Res.* **75,** 76–81
25. Li, Y., and Tsien, R. W. (2012) pHTomato, a red, genetically encoded indicator that enables multiplex interrogation of synaptic activity. *Nat. Neurosci.* **15,** 1047–1053
26. Collot, M., Loukou, C., Yakovlev, A. V., Wilms, C. D., Li, D., Evrard, A., Zamaleeva, A., Bourdieu, L., Léger, J. F., Ropert, N., Eilers, J., Oheim, M., Feltz, A., and Mallet, J. M. (2012) Calcium rubies. A family of red-emitting functionalizable indicators for two-photon Ca^{2+} imaging. *J. Am. Chem. Soc.* **134,** 14923–14931
27. Wu, J., Liu, L., Matsuda, T., Zhao, Y., Rebane, A., Drobizhev, M., Chang, Y. F., Araki, S., Arai, Y., March, K., Hughes, T. E., Sagou, K., Miyata, T., Nagai, T., Li, W. H., and Campbell, R. E. (2013) Improved orange and red Ca^{2+} indicators and photophysical considerations for optogenetic applications. *ACS Chem. Neurosci.* **4,** 963–972
28. McLachlan, J. (1960) The culture of *Dunaliella tertiolecta* Butcher. A euryhaline organism. *Can. J. Microbiol.* **6,** 367–379
29. Feldbauer, K., Zimmermann, D., Pintschovius, V., Spitz, J., Bamann, C., and Bamberg, E. (2009) Channelrhodopsin-2 is a leaky proton pump. *Proc. Natl. Acad. Sci. U.S.A.* **106,** 12317–12322
30. Cherny, V. V., Murphy, R., Sokolov, V., Levis, R. A., and DeCoursey, T. E. (2003) Properties of single voltage-gated proton channels in human eosinophils estimated by noise analysis and by direct measurement. *J. Gen. Physiol.* **121,** 615–628
31. Gray, P. (1994) Analysis of whole cell currents to estimate the kinetics and amplitude of underlying unitary events. Relaxation and "noise" analysis, in *Microelectrode Techniques: The Plymouth Workshop Handbook* (Ogden, D. C., ed) pp. 189–207, Company of Biologists, Cambridge, UK
32. Lois, C., Hong, E. J., Pease, S., Brown, E. J., and Baltimore, D. (2002) Germline transmission and tissue-specific expression of transgenes delivered by lentiviral vectors. *Science* **295,** 868–872
33. Hou, S. Y., Govorunova, E. G., Ntefidou, M., Lane, C. E., Spudich, E. N., Sineshchekov, O. A., and Spudich, J. L. (2012) Diversity of *Chlamydomonas* channelrhodopsins. *Photochem. Photobiol.* **88,** 119–128
34. Wang, J., Sasaki, J., Tsai, A. L., and Spudich, J. L. (2012) HAMP domain signal relay mechanism in a sensory rhodopsin-transducer complex. *J. Biol. Chem.* **287,** 21316–21325
35. Wang, W.-W., Sineshchekov, O. A., Spudich, E. N., and Spudich, J. L. (2003) Spectroscopic and photochemical characterization of a deep ocean proteorhodopsin. *J. Biol. Chem.* **278,** 33985–33991
36. Sineshchekov, O. A., Trivedi, V. D., Sasaki, J., and Spudich, J. L. (2005) Photochromicity of *Anabaena* sensory rhodopsin, an atypical microbial receptor with a *cis*-retinal light-adapted form. *J. Biol. Chem.* **280,** 14663–14668
37. Nack, M., Radu, I., Bamann, C., Bamberg, E., and Heberle, J. (2009) The retinal structure of channelrhodopsin-2 assessed by resonance Raman spectroscopy. *FEBS Lett.* **583,** 3676–3680
38. Sineshchekov, O. A., Govorunova, E. G., Jung, K.-H., Zauner, S., Maier, U.-G., and Spudich, J. L. (2005) Rhodopsin-mediated photoreception in cryptophyte flagellates. *Biophys. J.* **89,** 4310–4319
39. Kreimer, G. (1994) Cell biology of phototaxis in flagellate algae. *Int. Rev. Cytol.* **148,** 229–310
40. Govorunova, E. G., Spudich, E. N., Lane, C. E., Sineshchekov, O. A., and Spudich, J. L. (2011) New channelrhodopsin with a red-shifted spectrum and rapid kinetics from *Mesostigma viride*. *mBio* **2,** e00115–00111
41. Berthold, P., Tsunoda, S. P., Ernst, O. P., Mages, W., Gradmann, D., and Hegemann, P. (2008) Channelrhodopsin-1 initiates phototaxis and photophobic responses in *Chlamydomonas* by immediate light-induced depolarization. *Plant Cell* **20,** 1665–1677
42. Halldal, P. (1958) Action spectra of phototaxis and related problems in *Volvocales*, *Ulva* gametes and *Dinophyceae*. *Physiol. Plantarum* **11,** 118–153
43. Kato, H. E., Zhang, F., Yizhar, O., Ramakrishnan, C., Nishizawa, T., Hirata, K., Ito, J., Aita, Y., Tsukazaki, T., Hayashi, S., Hegemann, P., Maturana, A. D., Ishitani, R., Deisseroth, K., and Nureki, O. (2012) Crystal structure of the channelrhodopsin light-gated cation channel. *Nature* **482,** 369–374
44. Zhang, F., Vierock, J., Yizhar, O., Fenno, L. E., Tsunoda, S., Kianianmomeni, A., Prigge, M., Berndt, A., Cushman, J., Polle, J., Magnuson, J., Hegemann, P., and Deisseroth, K. (2011) The microbial opsin family of optogenetic tools. *Cell* **147,** 1446–1457
45. Tsunoda, S. P., and Hegemann, P. (2009) Glu 87 of channelrhodopsin-1 causes pH-dependent color tuning and fast photocurrent inactivation. *Photochem. Photobiol.* **85,** 564–569
46. Wang, H., Sugiyama, Y., Hikima, T., Sugano, E., Tomita, H., Takahashi, T., Ishizuka, T., and Yawo, H. (2009) Molecular determinants differentiating photocurrent properties of two channelrhodopsins from *Chlamydomonas*. *J. Biol. Chem.* **284,** 5685–5696
47. Sauvé, R., and Szabo, G. (1985) Interpretation of 1/f fluctuations in ion conducting membranes. *J. Theor. Biol.* **113,** 501–516
48. Berndt, A., Prigge, M., Gradmann, D., and Hegemann, P. (2010) Two open states with progressive proton selectivities in the branched channelrhodopsin-2 photocycle. *Biophys. J.* **98,** 753–761
49. Honig, B., Greenberg, A. D., Dinur, U., and Ebrey, T. G. (1976) Visual-pigment spectra. Implications of the protonation of the retinal Schiff base. *Biochemistry* **15,** 4593–4599
50. Subramaniam, S., Marti, T., and Khorana, H. G. (1990) Protonation state of Asp (Glu)-85 regulates the purple-to-blue transition in bacteriorhodopsin mutants Arg-82 → Ala and Asp-85 → Glu. The blue form is inactive in proton translocation. *Proc. Natl. Acad. Sci. U.S.A.* **87,** 1013–1017
51. Marti, T., Rösselet, S. J., Otto, H., Heyn, M. P., and Khorana, H. G. (1991) The retinylidene Schiff base counterion in bacteriorhodopsin. *J. Biol. Chem.* **266,** 18674–18683
52. Gergely, C., Ganea, C., Száraz, S., and Váró, G. (1995) Charge motions studied in the bacteriorhodopsin mutants D85N and D212N. *J. Photochem. Photobiol. B Biol.* **27,** 27–32
53. Gunaydin, L. A., Yizhar, O., Berndt, A., Sohal, V. S., Deisseroth, K., and Hegemann, P. (2010) Ultrafast optogenetic control. *Nat. Neurosci.* **13,** 387–392
54. Bamann, C., Kirsch, T., Nagel, G., and Bamberg, E. (2008) Spectral characteristics of the photocycle of channelrhodopsin-2 and its implication for

channel function. *J. Mol. Biol.* **375,** 686–694
55. Ritter, E., Stehfest, K., Berndt, A., Hegemann, P., and Bartl, F. J. (2008) Monitoring light-induced structural changes of Channelrhodopsin-2 by UV-visible and Fourier transform infrared spectroscopy. *J. Biol. Chem.* **283,** 35033–35041
56. Takahashi, T., Yan, B., Mazur, P., Derguini, F., Nakanishi, K., and Spudich, J. L. (1990) Color regulation in the archaebacterial phototaxis receptor phoborhodopsin (sensory rhodopsin II). *Biochemistry* **29,** 8467–8474
57. Pettei, M. J., Yudd, A. P., Nakanishi, K., Henselman, R., and Stoeckenius, W. (1977) Identification of retinal isomers isolated from bacteriorhodopsin. *Biochemistry* **16,** 1955–1959
58. Ohno, K., Takeuchi, Y., and Yoshida, M. (1977) Effect of light-adaptation on the photoreaction of bacteriorhodopsin from *Halobacterium halobium*. *Biochim. Biophys. Acta* **462,** 575–582
59. Verhoefen, M. K., Bamann, C., Blöcher, R., Förster, U., Bamberg, E., and Wachtveitl, J. (2010) The photocycle of channelrhodopsin-2. Ultrafast reaction dynamics and subsequent reaction steps. *Chemphyschem* **11,** 3113–3122
60. Suzuki, T., Yamasaki, K., Fujita, S., Oda, K., Iseki, M., Yoshida, K., Watanabe, M., Daiyasu, H., Toh, H., Asamizu, E., Tabata, S., Miura, K., Fukuzawa, H., Nakamura, S., and Takahashi, T. (2003) Archaeal-type rhodopsins in *Chlamydomonas*. Model structure and intracellular localization. *Biochem. Biophys. Res. Commun.* **301,** 711–717
61. Kianianmomeni, A., Stehfest, K., Nematollahi, G., Hegemann, P., and Hallmann, A. (2009) Channelrhodopsins of *Volvox carteri* are photochromic proteins that are specifically expressed in somatic cells under control of light, temperature, and the sex inducer. *Plant Physiol.* **151,** 347–366
62. Spudich, J. L., Yang, C.-S., Jung, K.-H., and Spudich, E. N. (2000) Retinylidene proteins. Structures and functions from archaea to humans. *Annu. Rev. Cell Dev. Biol.* **16,** 365–392
63. Gradmann, D., Berndt, A., Schneider, F., and Hegemann, P. (2011) Rectification of the channelrhodopsin early conductance. *Biophys. J.* **101,** 1057–1068
64. Ruffert, K., Himmel, B., Lall, D., Bamann, C., Bamberg, E., Betz, H., and Eulenburg, V. (2011) Glutamate residue 90 in the predicted transmembrane domain 2 is crucial for cation flux through channelrhodopsin 2. *Biochem. Biophys. Res. Commun.* **410,** 737–743
65. Plazzo, A. P., De Franceschi, N., Da Broi, F., Zonta, F., Sanasi, M. F., Filippini, F., and Mongillo, M. (2012) Bioinformatic and mutational analysis of channelrhodopsin-2 cation conducting pathway. *J. Biol. Chem.* **287,** 4818–4825
66. Richards, R., and Dempski, R. E. (2012) Re-introduction of transmembrane serine residues reduce the minimum pore diameter of channelrhodopsin-2. *PLoS One* **7,** e50018
67. Ullrich, S., Gueta, R.,and Nagel, G. (2013) Degradation of channelopsin-2 in the absence of retinal and degradation resistance in certain mutants. *Biol. Chem.* **394,** 271–280
68. Nagel, G., Brauner, M., Liewald, J. F., Adeishvili, N., Bamberg, E., and Gottschalk, A. (2005) Light activation of channelrhodopsin-2 in excitable cells of *Caenorhabditis elegans* triggers rapid behavioral responses. *Curr. Biol.* **15,** 2279–2284
69. Schroll, C., Riemensperger, T., Bucher, D., Ehmer, J., Völler, T., Erbguth, K., Gerber, B., Hendel, T., Nagel, G., Buchner, E., and Fiala, A. (2006) Light-induced activation of distinct modulatory neurons triggers appetitive or aversive learning in *Drosophila* larvae. *Curr. Biol.* **16,** 1741–1747
70. Brewer, G. J., Boehler, M. D., Jones, T. T., and Wheeler, B. C. (2008) NbActiv4 medium improvement to Neurobasal/B27 increases neuron synapse densities and network spike rates on multielectrode arrays. *J. Neurosci. Methods* **170,** 181–187